Available online at www.sciencedirect.com
ScienceDirect
Journal of the European Ceramic Society 27 (2007) 3081–3086
www.elsevier.com/locate/jeurceramsoc

Microwave dielectric properties and Far-infrared spectroscopic analysis of $Ba_{5+n}Ti_nNb_4O_{15+3n}$ $(0.3 < n < 1.2)$ ceramics

In-Sun Cho [a], Jeong-Ryeol Kim [a], Dong Wook Kim [a], Dong-Wan Kim [b], Kug Sun Hong [a,*]

[a] *School of Materials Science & Engineering, College of Engineering, Seoul National University, Shillim-dong, San 56-1, Gwanak-gu, Seoul 151-744, Republic of Korea*

[b] *Multifunctional Ceramics Research Center, Korea Institute of Science and Technology, Seoul 136-791, Republic of Korea*

Available online 9 January 2007

Abstract

$Ba_{5+n}Ti_nNb_4O_{15+3n}$ ceramics $(0.3 < n < 1.2)$ with a cation deficient hexagonal perovskite related structure were prepared by a conventional solid-state reaction method. The crystal structure and microstructure were investigated by X-ray powder diffraction (XRD) and field emission scanning electron microscope (FE-SEM), respectively. The microwave dielectric properties were measured using a network analyzer. The dielectric constant (ε_r) and the temperature coefficient of resonant frequency (τ_f) were increased and the quality factor ($Q \times f$) was decreased with increasing in the n value. The effect of the crystal structure on the microwave dielectric properties was also investigated. The FT-IR reflection spectra were obtained and analyzed using a Kramers–Kronig relation.

Keywords: Dielectric properties; Spectroscopy; Kramers–Kronig method; Niobates

1. Introduction

The rapid advances during the past decades in the microwave integrated circuit technology have brought a revolution in mobile communication and satellite broadcasting system. Several types of microwave dielectric materials such as $BaTi_4O_9$, $Ba_2Ti_9O_{20}$, $(Zr,Sn)TiO_4$ complex perovskite and $BaO–Nd_2O_3–TiO_2$ have been developed and put into practical use for microwave filters, dielectric resonators and patch antennas.[1–4] Comprehensive studies for new dielectric materials are required in order to improve various physical, chemical and dielectric properties of the dielectric resonators (DRs). For the application as DRs, the important dielectric properties required are high dielectric constant (ε_r) for miniaturization, high quality factor ($Q \times f$) for decrease of loss and small temperature coefficient of the resonant frequency (τ_f) for the temperature stability.[5] Recently, DRs with relative permittivity in the range of 40–54 have been reported in the system such as $Ba_5Nb_4O_{15}$ and $BaO–TiO_2–Nb_2O_5$.[6,7] Ratheesh et al. reported the dielectric properties of $BaTi_3Nb_4O_{17}$ and $Ba_6Ti_{14}Nb_2O_{39}$ in the microwave frequency region.[8] Furthermore, Fang et al. reported the microwave dielectric properties of cation-deficient hexagonal perovskites $Ba_{5+n}Ti_nNb_4O_{15+3n}$ $(n = 1, 2, 3)$ system.[9] The crystal structure of cation-deficient hexagonal perovskite type materials $Ba_{5+n}Ti_nNb_4O_{15+3n}$ have been studied by some authors through the Rietveld refinement method and TEM analysis. According to Duivenboden et al. $Ba_6TiNb_4O_{18}$ $(n = 1)$ consists of a framework of close-packed BaO_3 layers, 18R $(hhcccc)_3$.[10] According to Teneze et al. $Ba_{11}TiNb_8O_{33}$ $(n = 0.5)$ have a 33R stacking sequence of the BaO_3 layers leading to the cell parameters $a = 5.78634(2)$ Å, $c = 77.8011(4)$ Å with a space group $R\bar{3}m$.[11]

In the present study, the crystal structure and the microwave dielectric properties of $Ba_{5+n}Ti_nNb_4O_{15+3n}$ $(0.3 < n < 1.2)$ system were investigated. The Far-infrared reflectivity spectra were also measured and analyzed using the Kramers–Kornig (K–K) integration method for the survey of the dielectric loss ($\tan\delta$) in the microwave region.

2. Experimental procedure

The $Ba_{5+n}Ti_nNb_4O_{15+3n}$ $(n = 0.3, 0.5, 0.6, 0.7, 0.9, 1.0, 1.2)$ ceramics were prepared by the conventional solid-state reaction

* Corresponding author. Tel.: +82 2 880 8024; fax: +82 2 886 4156.
E-mail address: kshongss@plaza.snu.ac.kr (K.S. Hong).

0955-2219/$ – see front matter © 2007 Published by Elsevier Ltd.
doi:10.1016/j.jeurceramsoc.2006.11.030

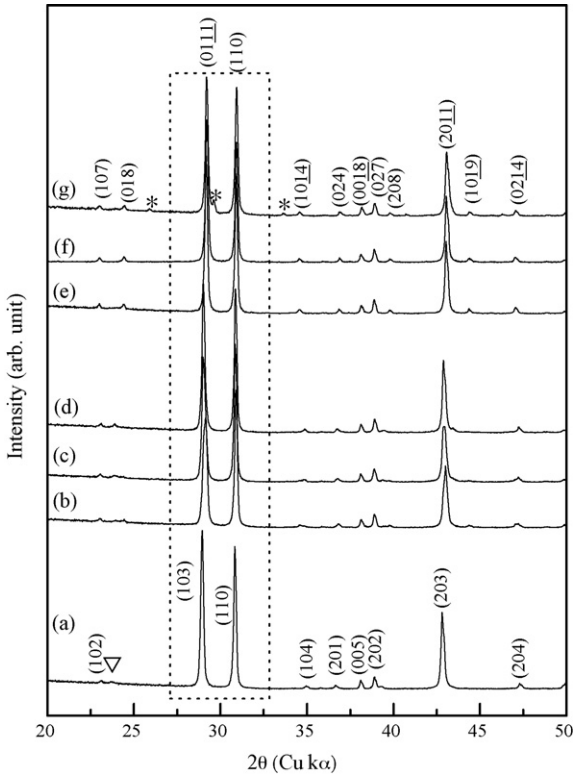

Fig. 1. The XRD patterns of $Ba_{5+n}Ti_nNb_4O_{15+3n}$ samples sintered at 1400 °C for (a) $n = 0.3$, (b) $n = 0.5$, (c) $n = 0.6$, (d) $n = 0.7$, (e) $n = 0.9$, (f) $n = 1.0$ and (g) $n = 1.2$. (*: BTN834, ▽: BTN1118).

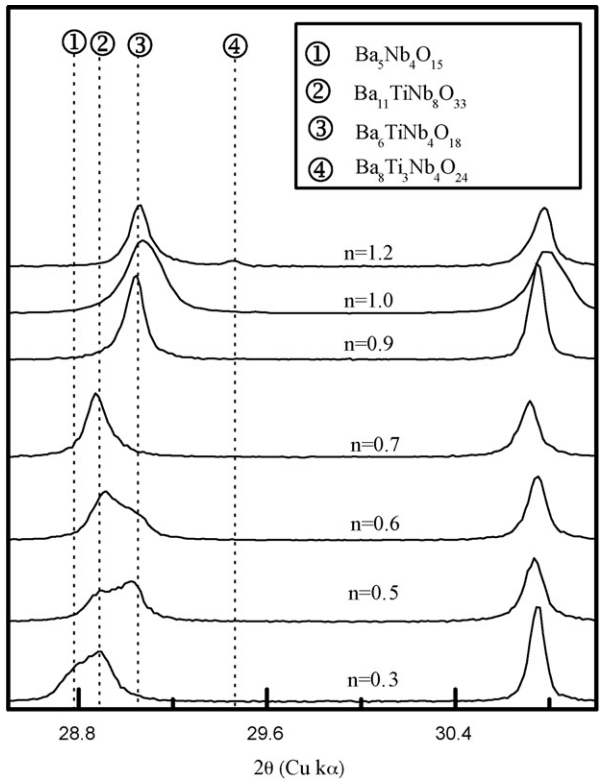

Fig. 2. The magnified view of the XRD patterns of $Ba_{5+n}Ti_nNb_4O_{15+3n}$ samples sintered at 1400 °C (main peak region between 28.5° and 31°).

method using high-purity $BaCO_3$ (99.9%), Nb_2O_5 (99.9%) and Rutile-TiO_2 (99.9%). The stoichiometric mixtures, after milling for 24 h using de-ionized water as a medium, were dried and calcined at 1300–1400 °C for 2 h. The calcined powders were thoroughly ground and ball-milled for 24 h. The milled powders were then dried, granulated, and pressed at 1000 kg/cm^2 to form pellets with an 8 mm diameter and 4 mm thick. The pellets were sintered at 1375–1400 °C with a heating rate of 5 °C/min. The densities of the sintered samples were measured by the Archimedes method.

The phase constitution and crystal structure of sintered samples were investigated by X-ray powder diffraction (Model D8_Advance, Bruker, Japan) using Cu Kα radiation (Ge monochromator) in the 2θ range from 10° to 90° (0.0137° step size). IR reflectance spectra were recorded using a Fourier-transform spectrometer (Bruker IFs 66 V/S) equipped with a fixed-angle specular reflectance accessory (external incidence angle of 11.5°). The surfaces of the sintered specimens were examined using field emission scanning electron microscopy (FESEM: Model JSM-6330F, JEOL, Japan). The microwave dielectric properties of the sintered samples were measured at microwave range using a network analyzer (Model HP8720C, Hewlett Packard, Palo Alto, CA).

3. Results and discussion

3.1. Structure analysis

The XRD patterns of $Ba_{5+n}Ti_nNb_4O_{15+3n}$ ($n = 0.3$, 0.5, 0.6, 0.7, 0.9, 1.0, 1.2) samples sintered at 1400 °C were shown in Fig. 1. The magnified view of rectangular region is shown in Fig. 2. The pattern for $n = 0.3$ sample (BTN03) was indexed based on the $Ba_5Nb_4O_{15}$ (B5N4) and

Table 1
Phase constituents and bulk densities of $Ba_{5+n}TinNb_4O_{15+3n}$ samples

n	Sintering temperature (°C)	Phase	Phase constituents	Bulk density (g/cm^3)
0.3	1400	Mixture	B5N4 + BTN1118	6.008
0.5	1400	Mixture	BTN1118 + BTN614	6.085
0.6	1400	Mixture	BTN1118 + BTN614	6.026
0.7	1400	Single phase	BTN1118	6.024
0.9	1400	Single phase	BTN614	6.109
1.0	1400	Single phase	BTN614	6.018
1.2	1400	Mixture	BTN614 + BTN834	6.070

B5N4, $Ba_5Nb_4O_{15}$; BTN1118, $Ba_{11}TiNb_8O_{33}$; BTN614, $Ba_6TiNb_4O_{18}$; BTN 834, $Ba_8Ti_3Nb_4O_{24}$.

showed additional reflection of second phase ($Ba_{11}TiNb_8O_{33}$ phase).

In the case of $n = 0.5$ (BTN05) and 0.6 (BTN06) samples, the patterns exhibited a mixture of $Ba_{11}TiNb_8O_{33}$ (BTN1118) and $Ba_6TiNb_4O_{18}$ (BTN614) phases. Moreover, the reflection intensity of the BTN1118 was increased and that of the BTN614 was decreased for $n = 0.6$ sample, which means the phase fraction of the BTN1118 is increased. Teneze et al., reported the

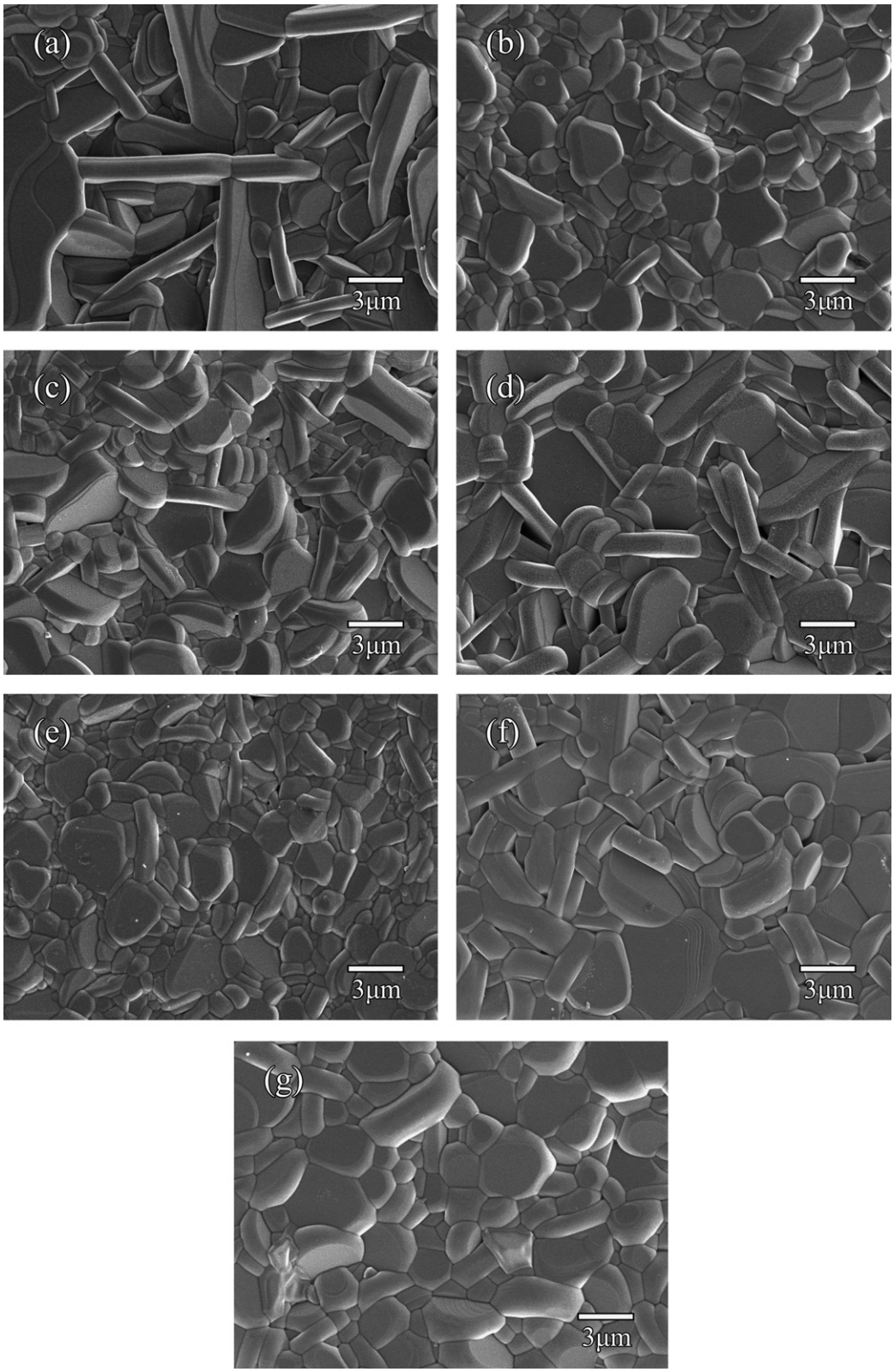

Fig. 3. The FE-SEM micrographs of $Ba_{5+n}Ti_nNb_4O_{15+3n}$ samples sintered at 1400 °C: (a) $n = 0.3$, (b) $n = 0.5$, (c) $n = 0.6$, (d) $n = 0.7$, (e) $n = 0.9$, (f) $n = 1.0$ and (g) $n = 1.2$.

$Ba_{11}TiNb_8O_{33}$ structure from the Rietveld refinement study and the $Ba_{11}TiNb_8O_{33}$ phase exist as the intergrowth compound between the $Ba_5Nb_4O_{15}$ and the $Ba_6TiNb_4O_{18}$.

For $n = 0.7$ (BTN07) sample, the BTN614 phase has disappeared and exhibited single phase hexagonal perovskite, $Ba_{11}TiNb_8O_{33}$. On the other hand, the XRD patterns of $n = 0.9$ (BTN09) and 1.0 (BTN10) samples are in agreement with the earlier report BTN614 phase (JCPDS No. 77-1786). All the peaks are indexed for the BTN614 phase and reflection of any second phase was not observed. Additionally, it is worth to note that the BTN12 ($n = 1.2$) sample was a mixture of two phases. The major phase is consistent with the $Ba_6TiNb_4O_{18}$, while the second phase (marked with asterisks in Fig. 1) is the $Ba_8Ti_3Nb_4O_{24}$ (BTN834) phase.

The phase constituents and bulk densities of sintered samples are summarized in Table 1. The measured bulk densities varied from 6.008 to 6.109 and the BTN09 samples has the maximum density value.

Microstructures of the sintered samples are shown in Fig. 3. The shape of the grains is not significantly varied and presents a disk-type morphology in all cases. The grain size of the BTN03 sample, however, is larger than the other samples. As can be seen in Fig. 3(b)–(f), the BTN09 ($n = 0.9$) sample has the smallest grains and a dense microstructure, which is coincident with the measured bulk densities.

3.2. Microwave dielectric properties

The microwave dielectric properties of $Ba_{5+n}Ti_nNb_4O_{15+3n}$ ($n = 0.3$–1.2) are shown in Fig. 4. The dielectric constant has a tendency of increase with increasing value of n, which is similar to the results of $Ba_nLa_4Ti_{3+n}O_{12+3n}$ ceramics reported by Okawa et al.[12] It is expected as the dielectric polarizability is increasing.[13] However, it is of interest that a deviation from the tendency of increase at $n = 0.5$ and 0.7 was observed. From the XRD analysis in Fig. 2, the BTN05 sample exhibited a mixture phase and has more fractions of the BTN614 phase. According to the results of Fang et al., the dielectric constant of the BTN614 is 48.9, which is higher than those of the BTN1118 (from our results at $n = 0.7$, $\varepsilon_r = 42.3$). Therefore, the larger value of dielectric constant of the BTN05 sample than the BTN07 is attributed to the decrease of the BTN614 phase fraction.

The quality factor ($Q \times f$) of $Ba_{5+n}Ti_nNb_4O_{15+3n}$ samples decreased linearly from 32,200 to 19,300 GHz with increasing n value. However, the BTN05 and the BTN07 samples have some deviation of this tendency of decrease such as the case of the dielectric constant. From the XRD analysis in Fig. 2, the BTN05 and BTN06 samples are mixtures of the BTN614 and the BTN1118 phase. The BTN614 phase (20,600 GHz) has a lower $Q \times f$ value than the BTN1118 phase (24,400 GHz). Therefore, the lower $Q \times f$ value of the BTN05 sample than the BTN07 is attributed to the small $Q \times f$ value of the BTN614 phase. It is well known that losses in microwave dielectrics consist of intrinsic and extrinsic components. The intrinsic loss is related to the crystal structure and bonding character of the materials. The extrinsic loss is mainly related to the defects, grain size and porosity, etc.[14] In order to examine the contribution of intrinsic loss component in the BTN05 and the BTN07 samples, FT-IR analysis was also conducted. As the n value increases from 0.3 to 1.0, the τ_f value is almost not changed but increases abruptly at $n = 1.2$. This abrupt increase of the τ_f value is attributed to the second phase of BTN834 ($\tau_f = +175$ ppm/°C).

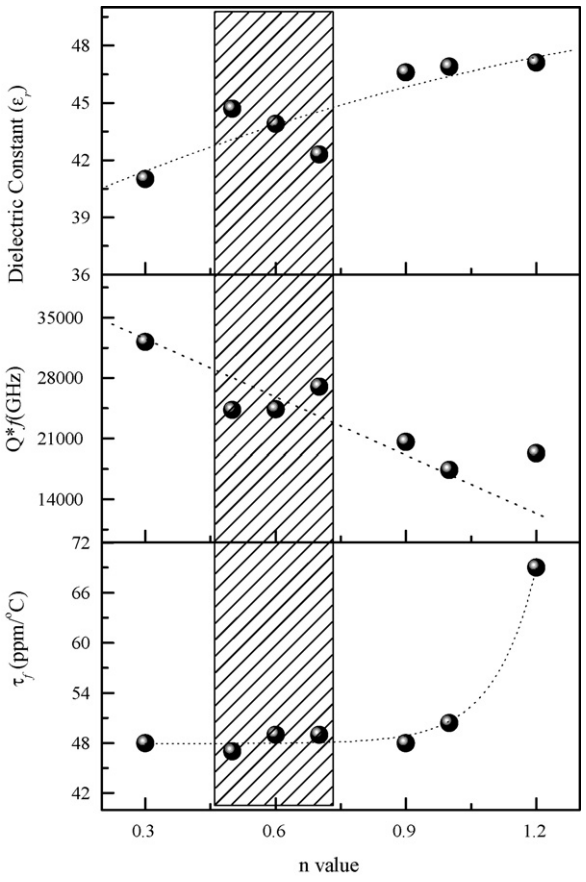

Fig. 4. The microwave dielectric properties of $Ba_{5+n}Ti_nNb_4O_{15+3n}$ sample as a function of n value.

3.3. FT-IR analysis

The Kramers–Kronig (K–K) analysis provides approximate dispersion parameters. The K–K transformation used in the evaluation of the reflectivity $R(\nu)$ may be written as:

$$\theta(\nu_m) = \frac{2\nu_m}{\pi} \int_0^\infty \frac{\ln\sqrt{R(\nu)}}{\nu^2 - \nu_m^2} \, d\nu \quad (1)$$

where $\theta(\nu_m)$ is phase angle at a specific frequency (ν_m) and ε' and ε'' can be obtained from:

$$n = \frac{1 - R}{1 - 2\sqrt{R}\cos\theta + R} \quad (2)$$

$$k = \frac{2\sqrt{R}\sin\theta}{1 - 2\sqrt{R}\cos\theta + R} \quad (3)$$

$$\varepsilon' = n^2 - k^2 \quad (4)$$

$$\varepsilon'' = 2nk \quad (5)$$

Table 2
The 1st–4th TO mode oscillator parameters and the calculated dielectric loss of $Ba_{5+n}Ti_nNb_4O_{15+3n}$ samples for $n = 0.5$ and 0.7

Sample	Mode	Ω_{jTO}	γ_j	γ_j/Ω_{jTO}	Calculated[a] $\tan\delta_j$ ($\gamma_j\omega/\Omega_{jTO}^2$)	Measured $Q \times f$ ($\tan\delta$)
	1st	55.3480	10.290	0.1859	7.84×10^{-4}	
	2nd	83.1780	14.959	0.1798	5.05×10^{-4}	
$n = 0.5$	3rd	109.9800	25.9220	0.2356	5.05×10^{-4}	24,300 GHz (2.88×10^{-4})
	4th	130.5800	16.3830	0.1254	5.00×10^{-4}	
	Sum				2.01×10^{-3}	
	1st	59.9840	6.0570	0.1009	3.93×10^{-4}	
	2nd	83.9440	12.3580	0.1472	4.09×10^{-4}	
$n = 0.7$	3rd	106.0500	23.4850	0.2214	4.88×10^{-4}	27,000 GHz (2.59×10^{-4})
	4th	129.7700	20.3490	0.1568	2.82×10^{-4}	
	Sum				1.57×10^{-3}	

[a] Calculated at 7 GHz from FT-IR data.

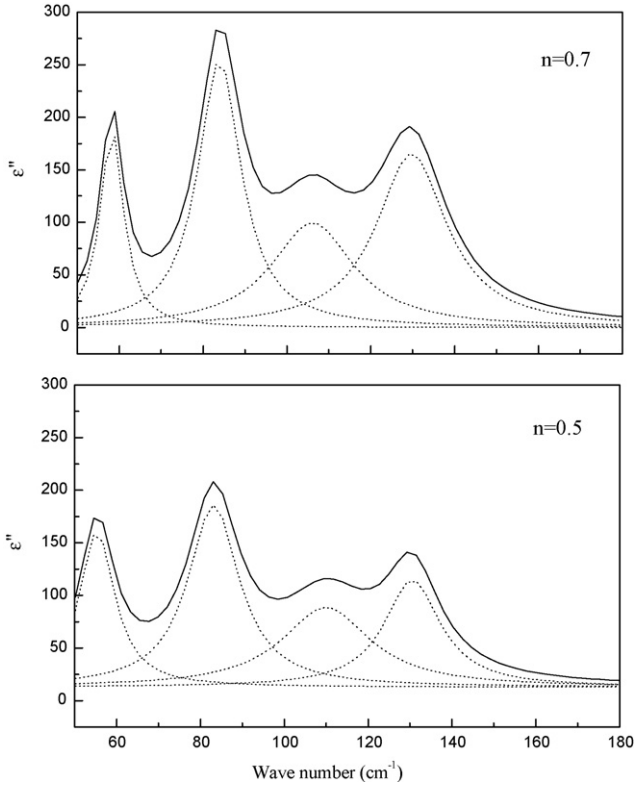

Fig. 5. Imaginary part of the dielectric constant and lorentzian fitting curves of $Ba_{5+n}Ti_nNb_4O_{15+3n}$ sample for $n = 0.5$ and 0.7.

where n is the index of refraction and k is the extinction coefficient.

The measured reflection spectra were transformed to the real and imaginary parts of the complex dielectric constant using the K–K transformation. The K–K integral is evaluated using Maclaurin's formula.[15] And the TO mode resonance peaks were obtained from ε'' spectra. Fig. 5 shows the calculated imaginary part of the complex dielectric constant and lorentzian fitting curves from 1st to 4th TO mode peaks.

According to the classical damped dispersion oscillator model, dielectric loss ($\tan\delta_j$) can be calculated from[16]:

$$\tan\delta_j = \frac{\Delta\varepsilon_j(\gamma_{jTO}\omega)/\Omega_{jTO}^2}{\varepsilon_\infty + \sum_k \Delta\varepsilon_k} \propto \frac{\gamma_{jTO}\omega}{\Omega_{jTO}^2} \quad (6)$$

where $\Delta\varepsilon_j$ is the oscillator strength, γ_{jTO} the damping constant and Ω_{jTO} is the transverse vibrational mode. The dielectric loss in the microwave region is mainly affected by the lowest TO modes in Far-IR region. In the approximation $\gamma_j/\Omega_{jTO} \ll 1$, the frequency of a given resonance, Ω_{jTO}, is the frequency at which ε'' is a maximum. Also γ_{jTO} is given by the frequency at which half-width of the ε'' peak.[17]

Since many phonon modes exist in the $Ba_{5+n}Ti_nNb_4O_{15+n}$ system, the calculation of the $\tan\delta$ becomes extremely complicated. In order to be easier to compare, the $\tan\delta$ between the samples of $n = 0.5$ and 0.7, the approximate $\tan\delta$ ($\sim\gamma_j 2\pi\nu_j/\Omega_{jTO}$) which is derived from Eq. (6) was used for the calculation. The calculated $\tan\delta$ value from the FT-IR data and the measured $\tan\delta$ (=$1/Q$) from the $Q \times f$ measurement are shown in Table 2. As can be seen that the calculated $\tan\delta$ from the FT-IR data looks to follow the measured data at microwave frequency, i.e. the calculated dielectric loss of the BTN05 sample was smaller than the BTN07 sample. However, we have to accumulate the FT-IR data for other samples to increase reliability of this estimation on the dielectric losses for this system.

4. Conclusion

$Ba_{5+n}Ti_nNb_4O_{15+3n}$ ceramics ($n = 0.3$, 0.5, 0.6, 0.7, 0.9, 1.0, 1.2) with cation deficient hexagonal perovskite related structure were prepared by the conventional solid-state reaction method. The phase constituents, microwave dielectric properties and FT-IR spectra have been investigated. With increasing n value, a mixture or a single phase appeared in the $Ba_{5+n}Ti_nNb_4O_{15+3n}$ system. The dielectric constant increased and the quality factor decreased linearly with increase in n value. However, in the region between $n = 0.5$ and 0.7, the deviation from linear tendency is observed. This deviation is explained by phase fraction difference of mixture. As the n value increased from 0.5 to 0.6, the fraction of the $Ba_6TiNb_4O_{18}$ phase decreased and that of the $Ba_{11}TiNb_8O_{33}$ phase was increased. The sample at $n = 0.7$ exhibited single phase of the $Ba_{11}TiNb_8O_{33}$. And the $Ba_{11}TiNb_8O_{33}$ phase had lower dielectric constant and higher $Q \times f$ value than the $Ba_6TiNb_4O_{18}$ phase. Thus, it is clear that the deviation from linear decrease at $n = 0.5$–0.7 was attributed to the increase of the $Ba_{11}TiNb_8O_{33}$ phase fraction.

In case of $n = 0.9$ and 1.0 sample, single phase of the $Ba_6TiNb_4O_{18}$ was appeared, and further increase from 1.0 to 1.2 caused formation of the $Ba_8Ti_3Nb_4O_{24}$ second phase. The Far-IR reflectivity was analyzed using K–K transformation and the dielectric loss was approximately calculated at $n = 0.5$ and 0.7. From the result of the K–K transformation, the $Ba_{11}TiNb_8O_{33}$ ($n = 0.7$) phase had the lower dielectric loss than the $Ba_6TiNb_4O_{18}$ phase. Furthermore, the $Ba_{11}TiNb_8O_{33}$ had a high dielectric constant of 42.3, a high quality factor 27,000 GHz and the τ_f of +47 ppm/°C.

Acknowledgement

This research was supported by a grant from the Center for Advanced Materials Processing (CAMP) of the 21st Century Frontier R&D Program funded by the Ministry of Commerce Industry and Energy (MOCIE), Republic of Korea.

References

1. Wersing, W., Microwave ceramics for resonators and filters. *Curr. Opin. Solid State Mater. Sci.*, 1996, **1**, 715–729.
2. Wolfran, G. and Gobel, H. E., Existence range, structural and dielectric properties of $Zr_xTi_ySn_zO_4$ ceramics ($x+y+z=2$). *Mater. Res. Bull.*, 1981, **16**, 1455–1463.
3. Ubic, R., Reaney, I. M. and Lee, W. E., Microwave dielectric solid-solution phase in system $BaO–Ln_2O_3–TiO_2$ (Ln = lanthanide cation). *Int. Mater. Rev.*, 1998, **43**, 205–219.
4. O'Bryan, H. M., Thomson, J. and Ploudre, J. K., A new $BaO–TiO_2$ compound with temperature-stable high permittivity and low microwave loss. *J. Am. Ceram. Soc.*, 1974, **57**, 450–453.
5. Kajfez, K. and Guillon, P., *Dielectric resonators*. Artech House, Massachsettus, 1986, p. 327.
6. Roberts, G. L., Cava, R. J., Peck, W. F. and Krajewski, J. J., Dielectric properties of barium titanium niobates. *J. Mater. Res.*, 1997, **12**, 526–530.
7. Sreemoolanadhan, H., Sebastian, M. T. and Mohanan, P., High permittivity and low loss ceramics in the $BaO–SrO–Nb_2O_5$ system. *Mater. Res. Bull.*, 1995, **30**, 653–658.
8. Ratheesh, R., Sreemoolanadhan, H., Suma, S., Sebastian, M. T., Jose, K. A. and Mohanan, P., New high permittivity and low loss ceramics in the $BaO–TiO_2–Nb_2O_5$ composition. *J. Mater. Sci. Mater. Electron.*, 1998, **9**, 291–294.
9. Fang, L., Chen, L., Zhang, H., Hong, X. K., Diao, C. L. and Liu, H. X., Microwave dielectric properties of $Ba_{5+n}Ti_nNb_4O_{15+3n}$ ceramics. *J. Mater. Sci. Mater. Electron.*, 2005, **16**, 149–151.
10. Boullay, P., Teneze, N., Trolliard, G., Mercurio, D. and Perez-Mato, J. M., Superpace description of the hexagonal perovskites in the system $Ba_5Nb_4O_{15}–BaTiO_3$ as modulated layered structure. *J. Solid State Chem.*, 2003, **174**, 209–220.
11. Teneze, N., Boullay, P., Trolliard, G. and Mercurio, D., The crystal structure of the intergrowth compound $Ba_{11}TiNb_8O_{33}$. *Solid State Sci.*, 2002, **4**, 1119–1128.
12. Okawa, T., Kiuchi, K., Okabe, H. and Ohsato, H., Microwave dielectric properties of $Ba_nLa_4Ti_{3+n}O_{12+3n}$ homologous series. *Jpn. J. Appl. Phys.*, 2001, **40**, 5779–5782.
13. Shannon, R. D., Dielectric polarizabilities of ions in oxides and fluorides. *J. Appl. Phys.*, 1993, **73**(1), 348–366.
14. Wakino, K. and Tamura, H., *Ceram. Trans.*, 1990, **8**, 305–314.
15. Ohta, K. and Ishida, H., Comparison among several numerical integration methods for Kramers–Kronig transformation. *Appl. Spectrosc.*, 1988, **42**, 952–957.
16. Fukuda, R., Kitoh, R. and Awai, I., Far-infrared reflection spectra of dielectric ceramics for microwave applications. *J. Am. Ceram. Soc.*, 1994, **77**(1), 149–154.
17. Spitzer, W. G., Miller, R. C., Dleinman, D. A. and Howarth, L. E., Far-infrared dielectric dispersion in $BaTiO_3$, $SrTiO_3$ and TiO_2. *Phys. Rev.*, 1962, **126**, 1710–1721.